Synthesis and characterisation of new Ni_2Mn, Ni_2Mn_2 and Mn_8 clusters by the use of 2-pyridyl oximes

Constantinos G. Efthymiou [a,b], Ioannis Mylonas-Margaritis [b], Sayak Das Gupta [c], Anastasios Tasiopoulos [d], Vassilios Nastopoulos [e], George Christou [c], Spyros P. Perlepes [e], Constantina Papatriantafyllopoulou [a,b,*]

[a] SSPC, Synthesis and Solid State Pharmaceutical Centre, Ireland
[b] School of Chemistry, National University of Ireland Galway, H91 TK 33 Galway, Ireland
[c] Department of Chemistry, University of Florida, Gainesville, FL 32611, United States
[d] Department of Chemistry, University of Cyprus, 1678 Nicosia, Cyprus
[e] Department of Chemistry, University of Patras, Patras 26504, Greece

ABSTRACT

The initial employment of methyl 2-pyridyl ketoxime, (py)C(Me)NOH, in mixed metal Ni/Mn cluster chemistry, provided access to complexes $[Ni_2^{II}Mn^{III}\{(py)C(Me)NO\}_6](ClO_4)$ (1) and $[Ni_2^{II}Mn_2^{III}\{(py)C(Me)NO\}_6(OMe)_2(MeOH)_2](ClO_4)_2$ (2) that display a linear and a *zig-zag* metal arrangement, respectively. 1 and 2 are synthesized by reacting $Ni(ClO_4)_2 \cdot 6H_2O$, (py)C(Me)NOH, $Mn(ClO_4)_2 \cdot 6H_2O$ and NaOMe in different molar ratios (2:6:1:6, 1; 1:3:1:3, 2) in MeOH, and they are the first examples of 3d–3d' mixed-metal clusters bearing (py)C(Me)NOH. The employment of phenyl 2-pyridyl ketoxime, (py)C(ph)NOH, instead of (py)C(Me) NOH, provided access to the octanuclear homometallic compound $[Mn_4^{II}Mn_4^{III}O_4(NO_3)_2\{(py)C(ph)NO\}_8(HCO_2)_2(MeOH)_2]$ (3) that possesses a double-butterfly $\{Mn_4^{II}Mn_4^{III}(\mu_4-O)_2(\mu_3-O)_2\}^{12+}$ core. 3 joins the small family of $Mn/(py)C(ph)NO^-$ clusters. Variable-temperature, solid-state *dc* and *ac* magnetic susceptibility studies were carried out on 1 and 2 and revealed the presence of antiferromagnetic exchange interactions between the metal ions ($J_{Mn-Ni} = -6.34 \pm 0.14$ cm^{-1} in 1; $J_{Mn-Ni} = -4.57 \pm 0.08$ cm^{-1}, $J_{Mn-Mn} = -12.72 \pm 0.12$ in 2) and a diamagnetic ground state for both compounds.

© 2019 Elsevier Ltd. All rights reserved.

1. Introduction

Metal clusters or polynuclear metal complexes are hybrid metal–organic species, in which multimetallic entities are held together through suitable organic ligands [1–3]. Their morphological features follow a general structural/architectural pattern, consisting of two distinct parts: (i) the inner metal core, M_xY_y (x = the number of metal ions M, y = the number of donor atoms of the ligands or anions, Y, that bridge the metal ions), the structural topology of which resembles with that of the minerals (oxides, chlorides, sulfides...), *and* (ii) the outer organic cell consisting of the aliphatic and/or aromatic parts of the ligands. The latter encapsulates the polar metal core, creating a hydrophobic protective environment. Thus, the metal clusters can be described alternatively as distinct fragments of infinite inorganic solids (minerals), such as oxides, possessing a zero dimensionality [4].

Metal clusters have become the focus of intense investigation over the last 30 years or so as they combine fascinating physical properties and intriguing geometrical features, being related to a variety of research fields including bioinorganic chemistry and molecular magnetism [5–14]. In the latter, the discovery that the compound $[Mn_{12}O_{12}(O_2CMe)_{16}(H_2O)_4]$ (Mn$_{12}$ac) could behave as a magnet at very low temperature, i.e. exhibiting single molecule magnetism (SMM) behaviour, stimulated a new era in the field of molecular nanomaterials [5–7]. This compound contains a mixed valence manganese oxide unit (Mn$_8^{III}$Mn$_4^{IV}$O$_{12}$), which is coordinated peripherally to twelve acetate ligands. The oxide fragment bears the properties, such as magnetism, of the bulk infinite oxides, and combine them with exotic properties at the nanoscale level, as quantum tunnelling of magnetization (QTM) and quantum phase interference, bridging the gap between the classical Newtonian and the quantum world. In addition to this, metal clusters with small magnetic anisotropy can be used as magnetic refrigerants, providing an efficient alternative to the use of helium-3 [8–10], whereas in the field of bioinorganic chemistry, they have been studied, amongst others, as models in order to elucidate details of the structure and function

of the active center of several metalloenzymes, such as ferritin, the Mn_4Ca water oxidizing complex in PSII, *etc* [11–14].

Various synthetic approaches have now been developed for the synthesis of metal clusters [2], with the vast majority of them including the use of bridging ligand(s), as it does not only dictate the metal topology and the molecular symmetry but also affects the magnetic, electronic, optical, *etc.* properties of the cluster. One family of ligands, that has been employed by us and others for the synthesis of new metal clusters, is the 2-pyridyl oximes (Scheme 1) [15–19]. The anions of such ligands are versatile and lead to the isolation of various clusters with interesting properties in a variety of research objectives, including single molecule magnetism, single-chain magnetism behaviour, *etc.* Our group recently reported two multiple-decker Ni_{12} and Ni_{16} molecular ferromagnets bearing the pyridine-2-aldoxime, that display high spin ground states $S = 6$ and $S = 8$, respectively, arising from ferromagnetic exchange interaction between the octahedral Ni^{II} ions [20,21]. We decided to expand our research efforts exploring the use of 2-pyridyl oxime ligands for the synthesis of mixed metal Ni/Mn clusters. The magnetic coupling between Ni^{II} and Mn^{III} is stronger than that between Mn^{II} and Mn^{III}, preventing complications from low-lying excited states in the analysis of the low-temperature magnetic susceptibility data [22]. In addition, although high nuclearity mixed-metal Mn^{III}–Ni^{II} complexes are relatively rare, they have the potential to yield species with unusually high nuclearities, such as the $Mn_{36}Ni_4$ "loop-of-loops-and-supertetrahedra" aggregate with $S = 26$ [23].

Herein, we report the synthesis and characterization of Ni_2Mn (**1**), Ni_2Mn_2 (**2**) and Mn_8 (**3**) species from the employment of methyl-2-pyridyl oxime (in **1** and **2**) and phenyl-2-pyridyl oxime (in **3**). **1** and **2** are the first examples of a 3d–3d′ heterometallic cluster bearing the methyl-2-pyridyl oxime; they exhibit antiferromagnetic exchange interactions between the metal centers that leads to a diamagnetic ground state.

2. Experimental

2.1. General and physical measurements

All manipulations were performed under aerobic conditions using materials (reagent grade) and solvents as received. (py)C(Me)NOH was prepared as previously described [24].

2.2. Compounds preparation

2.2.1. $[Ni_2Mn\{(py)C(Me)NO\}_6](ClO_4)$ (**1**)

$Ni(ClO_4)_2·6H_2O$ (0.366 g, 1.0 mmol), (py)C(Me)NOH (0.408 g, 3.0 mmol), $Mn(ClO_4)_2·6H_2O$ (0.145 g, 0.40 mmol) and NaOMe (0.162 g, 3.0 mmol) were dissolved in MeOH (25 mL). The resultant solution was stirred for 1 h at room temperature. Subsequently, a small quantity of red precipitate was removed by filtration and the dark red filtrate was allowed to stand undisturbed in a closed

R=H, Me, Ph, NH$_2$, CN...

Scheme 1. Structural formula of the family of 2-pyridyl oximes.

vial at room temperature. After 3 days, X-ray quality dark red block-shaped crystals of **1** were collected by filtration, washed with cold MeOH (2 × 2 mL) and dried under vacuum; the yield was 40%. The dried solid was analyzed satisfactorily as **1**. *Anal. Calc.* for **1**: C, 46.60; H, 3.91; N, 15.52. Found: C, 46.88; H, 3.52; N, 15.64%. Selected IR data (KBr, cm^{-1}): ṽ = 3400 (mb), 1624 (m), 1608 (m), 1590 (w), 1510 (w), 1490 (s), 1410 (m), 1280 (m), 1220 (m), 1190 (m), 1090 (s), 982 (m), 901 (m), 820 (m), 790 (m), 700 (s), 650 (m), 623 (s), 570 (m), 501 (m).

2.2.2. $[Ni_2Mn_2\{(py)C(Me)NO\}_6(OMe)_2(MeOH)_2](ClO_4)_2$ (**2**)

This complex was prepared in the same manner as complex **1** but by increasing the quantity of $Mn(ClO_4)_2·6H_2O$ (0.362 g, 1.00 mmol). Red prismatic crystals were formed within one day, and these were collected by filtration, washed with cold MeOH (2 × 2 mL) and dried under vacuum; the yield was 55%. The dried solid was hygroscopic and analyzed satisfactorily as **2**·$3H_2O$. *Anal. Calc.* for **2**·$3H_2O$: C, 38.99; H, 4.41; N, 11.86. Found: C, 39.42; H, 4.01; N, 11.39%. Selected IR data (KBr, cm^{-1}): ṽ = 3380 (mb), 1621 (m), 1583 (w), 1501 (w), 1478 (s), 1432 (m), 1296 (m), 1179 (m), 1112 (s), 989 (m), 908 (m), 813 (m), 776 (m), 708 (s), 635 (m), 623 (s), 558 (m), 490 (m).

2.2.3. $[Mn_8O_4(NO_3)_2\{(py)C(ph)NO\}_8(HCO_2)_2(MeOH)_2]$ (**3**)

Method A: $Ni(ClO_4)_2·6H_2O$ (0.040 g, 0.10 mmol), (py)C(ph)NOH (0.060 g, 0.30 mmol), $Mn(NO_3)_2·6H_2O$ (0.086 g, 0.30 mmol) and NaOMe (0.017 g, 0.30 mmol) were dissolved in CH_2Cl_2 (20 mL). The resultant yellowish solution was stirred for 24 h at room temperature, during which time its color turned to dark brown/black. Subsequently, a small quantity of brown precipitate was removed by filtration and the solution was layered with Et$_2$O (40 mL). Slow mixing gave well-formed, X-ray quality black crystals of the product, which were collected by filtration, washed with Et$_2$O (2 × 3 mL) and dried in air. Typical yields were in the 5–15% range. *Anal. Calc.* for **3**: C, 51.47; H, 3.64; N, 9.61. Found: C, 51.28; H, 3.87; N, 10.11%. Selected IR data (KBr, cm^{-1}): ṽ = 3445m, 2363m, 2344m, 1684m, 1653s, 1616w, 1508m, 1559s, 1453m, 1437m, 1384s, 1190w, 1100w, 1064m, 1029m, 791w, 744w, 709m, 600m, 462w.

*Method B:* Following the same procedure as in Method A, but in the absence of a Ni^{II} source, black, prismatic crystals of **3** were isolated in ~12% yield. The product was identified by IR spectral comparison with the authentic material.

2.3. Physical studies

Infrared spectra were recorded in the solid state (KBr pellets) on a Shimadzu Prestige-21 spectrometer in the 4000–400 cm^{-1} range. Variable-temperature dc and ac magnetic susceptibility data were collected at the University of Florida using a Quantum Design MPMS-XL SQUID susceptometer equipped with a 7 T magnet and operating in the 1.8–300 K range. Samples were embedded in solid eicosane to prevent torquing. The ac magnetic susceptibility measurements were performed in an oscillating ac field of 3.5 G and a zero dc field. The oscillation frequencies were in the 5–1488 Hz range. Pascal's constants were used to estimate the diamagnetic corrections, which were subtracted from the experimental susceptibilities to give the molar paramagnetic susceptibility (χ_M).

2.4. Single-crystal X-ray crystallography

Data were collected at the University of Cyprus on an Oxford-Diffraction Xcalibur-3 diffractometer, equipped with a CCD area detector and a graphite monochromator utilizing Mo Kα radiation (λ = 0.71073 Å). Suitable crystals for **1–3** were attached to glass fiber using paratone-N oil and transferred to a goniostat where
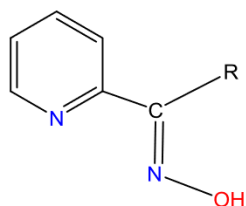
they were cooled to 100 K for data collection. Empirical absorption corrections (multi-scan based on symmetry-related measurements) were applied using CrysAlisRED software [25]. Software packages used: CrysAlisCCD for data collection, CrysAlisRED for cell refinement and data reduction [25], SHELXL for structure solution [25], WINGX for geometric calculations [26], while DIAMOND [27] and MERCURY [28] were used for molecular graphics. The program Squeeze [29], a part of the PLATON package of crystallographic software, was used to remove contribution of highly disordered solvate molecules in 2 and 3. The non-H atoms were treated anisotropically, whereas the H atoms were placed in calculated, ideal positions and refined as riding on their respective C atoms.

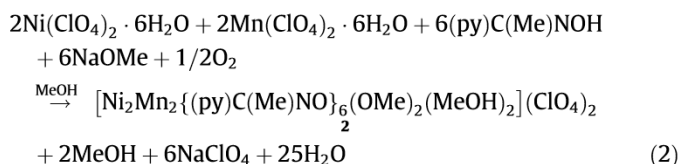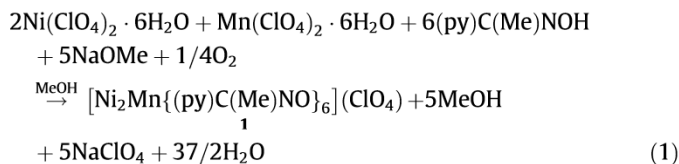Crystallographic data can be found in Table 1.

3. Results and discussion

3.1. Synthesis

Our groups have developed an intense interest in the employment 2-pyridyl oximes as a means for the isolation of metal clusters [20,21,30–35]. Such ligands have a rich coordination chemistry, bridging a large number of metals, thus resulting in the formation of high nuclearity species, whereas they often favor the ferromagnetic coupling between the metal centers. Our research efforts have yielded a variety of homometallic and 3d/4f mixed-metal species, including Ni_{12} [20], Ni_{16} [20,21], Ni_8Ln_8 [31], etc, examples. Wishing to expand this work, we aimed at the investigation of the previously unexplored $Ni^{II}/Mn^{III}/(py)C(Me)NOH$ reaction system, probing its potential to yield new 3d–3d′ mixed-metal clusters with interesting structural features and magnetic properties.

Various reactions have been systematically explored in the absence of carboxylates and other auxiliary ligands, with differing reagent ratios, reaction solvents and other conditions. The reaction of $Ni(ClO_4)_2\cdot6H_2O$, $(py)C(Me)NOH$, $Mn(ClO_4)_2\cdot6H_2O$ and NaOMe, in a 2:6:1:6 molar ratio, in MeOH, gave a dark red solution from which compound $[Ni_2Mn\{(py)C(Me)NO\}_6](ClO_4)$ (1) was subsequently isolated. Changing the molar ratio of the reactants to 1:3:1:3, i.e. increasing the quantity of the Mn^{II} ions that are present

in the reaction mixture, and following a similar procedure to the one that yielded 1, compound $[Ni_2Mn_2\{(py)C(Me)NO\}_6(OMe)_2(MeOH)_2](ClO_4)_2$ (2) was formed in good yield. The stoichiometric reactions that afforded compounds 1 and 2 are summarized in Eqs. (1) and (2).

$$2Ni(ClO_4)_2\cdot6H_2O + Mn(ClO_4)_2\cdot6H_2O + 6(py)C(Me)NOH + 5NaOMe + 1/4O_2$$
$$\overset{MeOH}{\rightarrow} [Ni_2Mn\{(py)C(Me)NO\}_6](ClO_4) + 5MeOH$$
$$+ 5NaClO_4 + 37/2H_2O \qquad (1)$$

$$2Ni(ClO_4)_2\cdot6H_2O + 2Mn(ClO_4)_2\cdot6H_2O + 6(py)C(Me)NOH + 6NaOMe + 1/2O_2$$
$$\overset{MeOH}{\rightarrow} [Ni_2Mn_2\{(py)C(Me)NO\}_6(OMe)_2(MeOH)_2](ClO_4)_2$$
$$+ 2MeOH + 6NaClO_4 + 25H_2O \qquad (2)$$

After the isolation of 1 and 2, which revealed that small changes in the Ni^{II}/Mn^{II} ratio yields different products, many other experiments were performed towards this direction. During these efforts, it was observed that by further decreasing the amount of Ni^{II} in the reaction mixture, a dark brown/black microcrystalline precipitate was formed. Efforts were then took place to grow single crystals by using different solvents, metal sources and bases; however, this was not feasible, so we decided to use $(py)C(ph)NOH$, hoping that the additional π–π interactions introduced by the phenyl rings, could potentially improve the crystallinity of the product. Indeed, the reaction of $Ni(ClO_4)_2\cdot6H_2O$, $(py)C(ph)NOH$, $Mn(NO_3)_2\cdot6H_2O$ and NaOMe, in a 1:3:3:3 molar ratio, in CH_2Cl_2, gave dark brown crystals of the homometallic compound $[Mn_8O_4(NO_3)_2\{(py)C(ph)NO\}_8(HCO_2)_2(MeOH)_2]$ (3) in a very low yield. After the determination of the crystal structure of 3, which revealed that the Ni^{II} ions do not participate in its formation, the synthesis of 3 was achieved by reacting equivalent quantities of $(py)C(ph)NOH$, $Mn(NO_3)_2\cdot6H_2O$ and NaOMe in CH_2Cl_2. Many experiments were also performed in order to improve the reaction yield; this has not been achieved, preventing the study of the magnetic properties of this compound. The synthesis of 3 is summarized in the stoichiometric Eq. (3). It is worth mentioning that a part of the MeO-ions, that were used to
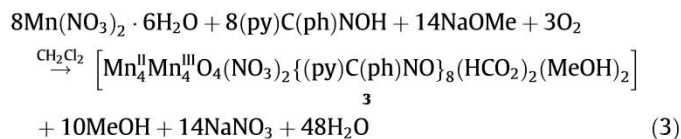
Table 1
Crystallographic data for complexes 1, 2, and 3.

Complex	1	2	3
Empirical formula	$C_{42}H_{42}ClMnN_{12}Ni_2O_{10}$	$C_{46}H_{56}Cl_2Mn_2N_{12}Ni_2O_{18}$	$C_{100}H_{80}Mn_8N_{18}O_{24}$
Formula weight	1082.68	1363.23	2357.34
Crystal system	trigonal	triclinic	monoclinic
Space group	R-3	$P\bar{1}$	$C\,2/c$
a (Å)	14.1458(6)	9.1751(6)	24.8584(8)
b (Å)	14.1458(6)	12.4211(10)	16.5098(6)
c (Å)	23.9250(8)	14.2957(13)	26.3028(11)
α (°)	90.00	87.503(7)	90
β (°)	90.00	88.130(7)	95.279(4)
γ (°)	120.00	79.355(6)	90
V (Å³)	4146.1(4)	1599.1(2)	10749.1(7)
Z	3	1	4
ρ_{calc} (g cm⁻³)	1.301	1.416	1.457
Radiation, λ (Å)	0.71073	0.71073	0.71073
μ (mm⁻¹)	1.006	1.121	0.986
T (K)	100(2)	100(2)	100(2)
Measured/independent reflections (R_{int})	11606/2301 (0.0182)	25161/6950 (0.0283)	29395/9152 (0.0699)
Parameters refined	143	405	688
Goodness of fit (GoF) (on F^2)	1.084	1.036	1.066
R_1[a] ($I > 2\sigma(I)$)	0.0566	0.0376	0.0813
wR_2[b]	0.1660	0.1087	0.2039
$(\Delta\rho)_{max}/(\Delta\rho)_{min}$ (e Å⁻³)	1.459/−0.431	0.609/−0.435	0.353/−0.213

[a] $R_1 = \Sigma(|F_o| - |F_c|)/\Sigma(|F_o|)$.
[b] $wR_2 = \{\Sigma[w(F_o^2 - F_c^2)^2]/\Sigma[w(F_o^2)^2]\}^{1/2}$, $w = 1/[\sigma^2(F_o^2) + (aP)^2 + bP]$, where $P = (F_o^2 + 2F_c^2)/3$ and a and b are the two weighting parameters suggested by the SHELXL refinement software.

deprotonate the ligand, have been oxidized to HCO_2^- during the aerial aggregation process [36] as small alkoxides are susceptible to air oxidation [37].

$$8Mn(NO_3)_2 \cdot 6H_2O + 8(py)C(ph)NOH + 14NaOMe + 3O_2$$

$$\xrightarrow{CH_2Cl_2} \left[Mn_4^{II}Mn_4^{III}O_4(NO_3)_2\{(py)C(ph)NO\}_8(HCO_2)_2(MeOH)_2 \right]_3$$

$$+ 10MeOH + 14NaNO_3 + 48H_2O \qquad (3)$$

3.2. Description of structures

Representations of the molecular structures and structural cores of complexes **1–3**, are shown in Figs. 1–3. Selected interatomic distances and angles for the three complexes are listed in Tables 2–4.

1 crystallizes in the trigonal space group R-3. Its crystal structure is composed of trinuclear $[Ni_2^{II}Mn^{III}\{(py)C(Me)NO\}_6]^+$ cations and ClO_4^- anions. The cationic complex possesses a C_{3i} symmetry and consists of two Ni^{II} and one Mn^{III} ions that are held together through six $\eta^1{:}\eta^1{:}\eta^1{:}\mu_2$ (py)C(Me)NO$^-$ ligands (Scheme 2) with the Ni–N_{ox} bond lengths [2.024 Å] being slightly shorter than the Ni–N_{py} ones [2.060 Å]. The structural core of the complex can be described as a linear heterometallic $\{Ni_2Mn(N\cap O)_6\}^+$ unit, where the six diatomic N∩O bridges are coming from six different oximate groups. Alternatively, the structure of **1** can be described as being constructed by two $[Ni\{(py)C(Me)NO\}_3]^-$ fragments, which are linked to a central Mn^{III} ion. This is a building block approximation and can be considered as a rational approach for interpreting, predicting and controlling the rather "serendipitous" metal cluster's assembly [38].

A principal C_3 axis passes through the three metal ions in **1**, while the Mn^{III} is located on an inversion center. The Ni^{II} ions are six-coordinate with distorted octahedral coordination sphere, which is completed by six N donor atoms, three pyridyl and three oximic in facial (fac−) arrangement. The coordination geometry around the Mn^{III} ion forms a nearly perfect octahedron with the six Mn–O bonds being equivalent as a consequence of the crystallographic symmetry in **1**. Hence, **1** is a conceptual model for the Pearson's Hard and Soft Acids and Bases (HSAB) theory, with the hard basic O donor atoms tending to coordinate to the higher oxidation Mn^{III} species, while the intermediate basicity N atoms showing a preference for the less acidic Ni^{II} ions.
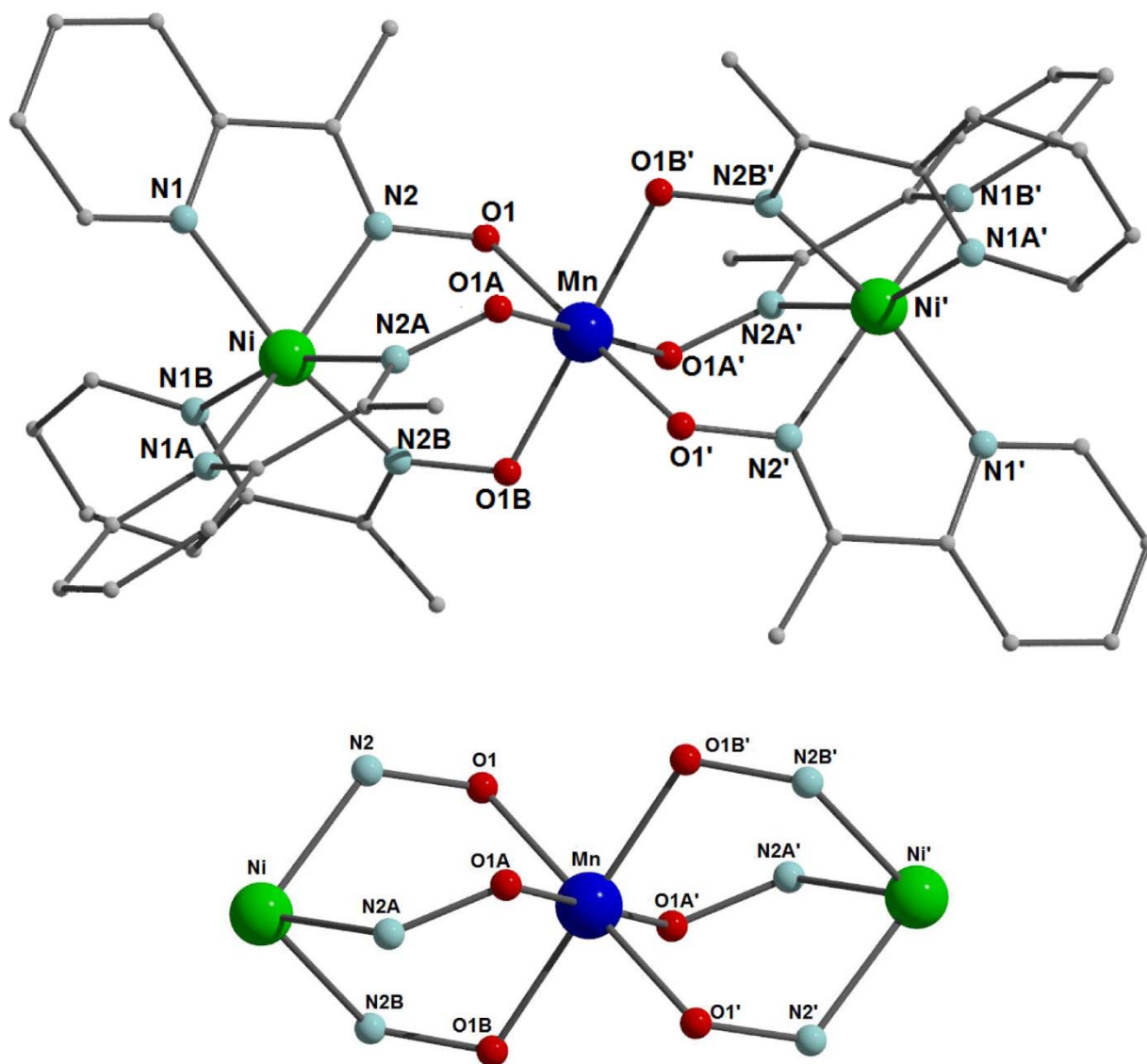

Fig. 1. Representation of the molecular structure of the cationic cluster **1** (top) and its $\{Ni_2Mn(N\cap O)_6\}^+$ structural core (bottom). Color code Mn^{III}, blue; Ni^{II}, green; O, red; N, aqua; C, grey. The hydrogen atoms and the ClO_4^- counteranions have been omitted for clarity. (Colour online.)
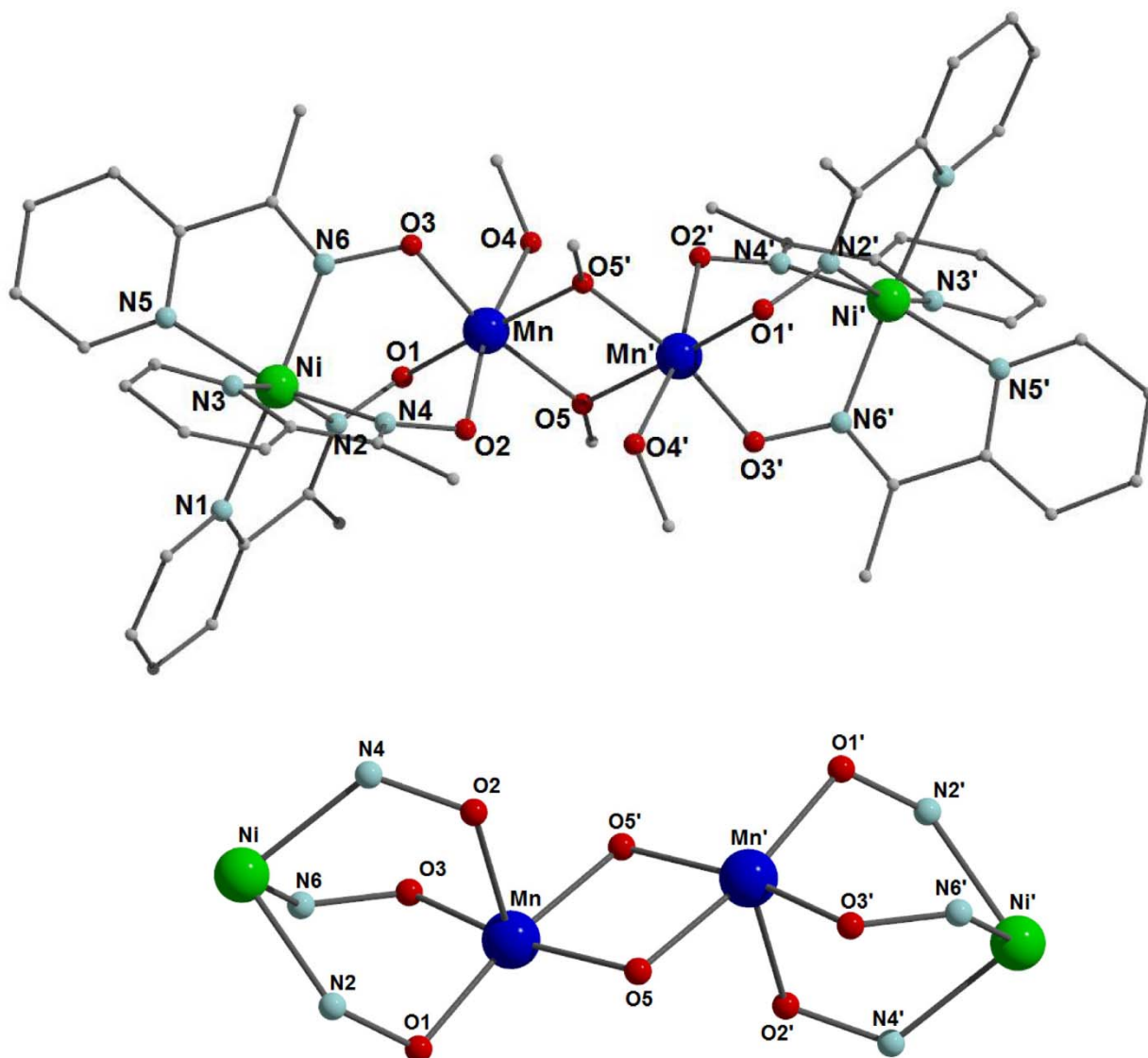
Fig. 2. Representation of the molecular structure of the cationic cluster **2** (top) and its structural core (bottom). Color code Mn^{III}, blue; Ni^{II}, green; O, red; N, aqua; C, grey. The hydrogen atoms and the ClO$_4^-$ counteranions have been omitted for clarity. (Colour online.)

The oxidation state of the Mn^{III} ion was confirmed by charge balance considerations and bond-valence sum (BVS) calculations [39]. The intracationic intermetallic distances are Ni$\cdots$Mn = 3.501 (1) Å and Ni$\cdots$Ni' = 7.002(1) Å; a close inspection shows that there are not significant inter- or intracationic hydrogen bonding interactions, and the cations are well-isolated with the shortest metal$\cdots$metal separation between the neighboring Ni$_2$Mn units being 8.225(2) Å (Ni$\cdots$Ni).

Cluster **2** crystallizes in the triclinic space group $P\bar{1}$. Its structure consists of a centrosymmetric [Ni$_2^{II}$Mn$_2^{III}${(py)C(Me)NO}$_6$ (OMe)$_2$(MeOH)$_2$]$^{2+}$ cation, and two ClO$_4^-$ ions. The four metal ions are held together through six η^1:η^1:η^1:μ_2 pyridyl oxime ligands (Scheme 2), and two μ-MeO$^-$ bridging ligands. They display a zig-zag arrangement with the two Mn^{III} ions being located at the center and the Ni^{II} ions on the outer part. The structure of **2** can be described as consisting of [Ni{(py)C(Me)NO}$_3$]$^-$ fragments, which are linked to a Mn^{III} ion, constructing an heterometallic [(Ni{(py)C(Me)NO}$_3$)Mn]$^{2+}$ unit; the dimerization of the latter through the μ-MeO$^-$ ions results in the formation of **2**.

All the metal ions in **2** ions display a distorted octahedral coordination geometry. The coordination environment around the Ni^{II}

ions consists of six N atoms, coming from three different (py)C(Me)NO$^-$ ligands, whereas the coordination sphere of the Mn^{III} ions is completed by three oximate O atoms, two methoxide O atoms and one terminal MeOH. The intracationic, intermetallic distances are Ni$\cdots$Mn = 3.489(1) Å, Mn–Mn' = 3.006(1) Å, and Ni$\cdots$Ni' = 9.611(1) Å; there are not strong inter- or intramolecular hydrogen bonding interactions in **2**, and the shortest metal$\cdots$metal distance between the neighboring Ni$_2$Mn$_2$ cations is 8.484(2) Å (Ni$\cdots$Mn).

The oxidation states of the Mn and the protonation level of the O atoms were confirmed by charge balance considerations and bond-valence sum (BVS) calculations [39], as well as the observation of Jahn–Teller distortions for the octahedral Mn^{III} ions, which take the form of axial elongation of the O2–Mn–O3 and the symmetry equivalent axes.

1 and **2** are the first 3d–3d' mixed-metal clusters bearing the neutral or anionic form of (py)C(Me)NOH. They also join a small family of 2-pyridyl oxime Ni/Mn complexes, the vast majority of which is based on 2-pyridyl aldoxime and its derivatives [40–48].

3 crystallizes in the monoclinic space group $C\,2/c$. Its structure consists of neutral [Mn$_8$O$_4$(NO$_3$)$_2${(py)C(ph)NO}$_8$(HCO$_2$)$_2$(MeOH)$_2$]
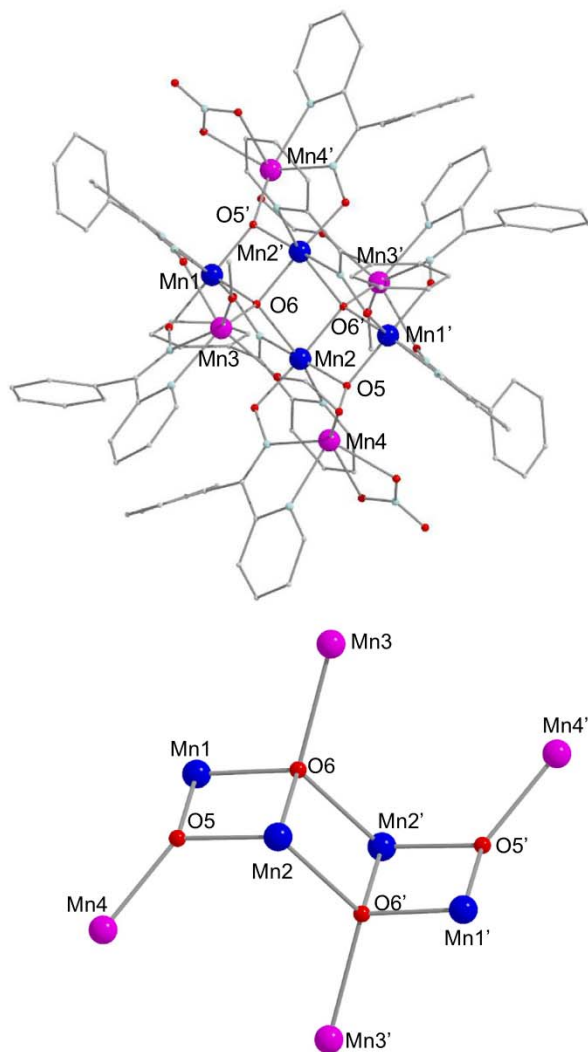
Fig. 3. Representation of the molecular structure of the cationic cluster **3** (top) and its structural core (bottom). Color code Mn^{III}, blue; Mn^{II}, violet; O, red; N, aqua; C, grey. The hydrogen atoms have been omitted for clarity. (Colour online.)

Table 2
Selected interatomic distances (Å) and angles (°) for **1**.

Interatomic distances (Å)			
Ni–N1	2.080(3)	Ni–N2B	2.015(3)
Ni–N1A	2.080(3)	Mn–O1	1.930(2)
Ni–N1B	2.080(3)	Mn–O1A	1.930(2)
Ni–N2	2.015(3)	Mn–O1B	1.930(2)
Ni–N2A	2.015(3)		
Bond angles (°)			
N1–Ni–N1A	95.0(1)	N2–Ni–N2A	87.1(1)
N1–Ni–N2	77.4(1)	O1–Mn–O1'	180.0(1)
N1–Ni–N2A	103.1(1)	O1–Mn–O1A	94.6(1)
N1–Ni–N2B	160.8(1)	O1–Mn–O1A'	85.4(1)
Ni–Mn	3.501(1)		

[a] Symmetry transformations used to generate equivalent atoms: (A): $-x + y, -x, z$; (B): $-y, x - y, z$; ('): $-x, -y, 1 - z$; (A'): $x - y, x, 1 - z$; (B'): $y, -x + y, 1 - z$.

Table 3
Selected interatomic distances (Å) and angles (°) for **2**.

| Interatomic distances (Å)			
Ni–N1	2.097(2)	Mn–O1	1.920(2)
Ni–N2	2.054(2)	Mn–O2	2.173(2)
Ni–N3	2.101(2)	Mn–O3	1.904(2)
Ni–N4	2.033(2)	Mn–O4	2.288(2)
Ni–N5	2.117(2)	Mn–O5	1.949(2)
Ni–N6	2.042(2)	Mn–O5'	1.946(2)
Ni–Mn	3.489(2)	Mn–Mn'	3.006(2)
Bond angles (°)			
N1–Ni–N2	77.2(1)	O1–Mn–O2	95.7(1)
N1–Ni–N3	92.4(1)	O1–Mn–O3	96.7(1)
N1–Ni–N4	99.5(1)	O1–Mn–O4	85.7(1)
N1–Ni–N5	94.3(1)	O1–Mn–O5	95.2(1)
N1–Ni–N6	159.7(1)	O1–Mn–O5'	171.2(1)
N2–Ni–N3	161.7(1)	O2–Mn–O3	96.2(1)
N2–Ni–N4	89.3(1)	O2–Mn–O4	169.2(1)
N2–Ni–N5	102.3(1)	O2–Mn–O5	86.2(1)
N2–Ni–N6	87.2(1)	O2–Mn–O5'	90.4(1)
N3–Ni–N4	77.4(1)	O3–Mn–O5	167.6(1)
N3–Ni–N5	93.4(1)	O3–Mn–O5'	89.0(1)
N3–Ni–N6	105.9(1)	O3–Mn–O4	94.3(1)
N4–Ni–N5	93.2(1)	O5–Mn–O5'	78.7(1)
N4–Ni–N5	163.7(1)	O4–Mn–O5	83.0(1)
N5–Ni–N6	76.1(1)	O4–Mn–O5'	87.2(1)

[a] Symmetry transformations used to generate equivalent atoms: $-x, 1 - y, 1 - z$.

Table 4
Selected interatomic distances (Å) and angles (°) for **3**.

Interatomic distances (Å)			
Mn1–O5	1.838(4)	Mn⋯Mn2'	3.260(4)
Mn1–O6	1.850(4)	Mn1⋯Mn4	3.641(4)
Mn2–O5	1.868(4)	Mn1⋯Mn3	3.343(4)
Mn2–O6	1.926(4)	Mn2⋯Mn3	3.643(4)
Mn2–O6'	2.311(5)	Mn2⋯Mn4	3.403(4)
Mn3–O6	2.248(5)	Mn3⋯Mn2'	3.896(4)
Mn4–O5	2.071(4)	Mn4⋯Mn2'	5.545(4)
Mn1⋯Mn2	2.789(5)		
Bond angles (°)			
O5–Mn1–O6	85.1(2)	Mn1–O6–Mn3	108.9(2)
O5–Mn2–O6	82.2(2)	Mn1–O6–Mn2'	111.6(2)
O5–Mn2–O6'	111.0(2)	Mn2–O5–Mn4	119.4(2)
O6–Mn2–O6'	79.8(2)	Mn2–O6–Mn3	121.3(2)
Mn1–O5–Mn2	97.6(2)	Mn2–O6–Mn2'	100.2(2)
Mn1–O5–Mn4	137.2(2)	Mn3–O6–Mn2'	117.4(2)
Mn1–O6–Mn2	95.2(2)		

[a] Symmetry transformations used to generate equivalent atoms: $-x + 1/2, -y + 1/2, -z + 1$.
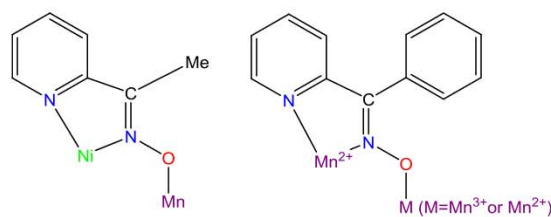
Scheme 2. The $\eta^1:\eta^1:\eta^1:\mu_2$ coordination mode of the organic ligands in **1**, **2** (left), and **3** (right).

cluster molecules. There are four Mn^{II} and four Mn^{III} ions that are held together through two μ_4-O^{2-} and two μ_3-O^{2-} ions, eight η^1:η^1:η^1:μ_2 (py)C(ph)NO$^-$ ligands (Scheme 2), and two μ_2-HCO$_2^-$ ions. The (py)C(ph)NO$^-$ ligands connect either two Mn^{III}, or one Mn^{II} with one Mn^{III} ions, whereas the HCO$_2^-$ ions bridge two Mn^{II} metal centers in a *syn-anti* fashion. **3** possesses a double-butterfly $\{Mn_4^{II}Mn_4^{III}(\mu_4\text{-}O)_2(\mu_3\text{-}O)_2\}^{12+}$ metal core, which is composed of two $\{Mn_2^{II}Mn_2^{III}(\mu_4\text{-}O)(\mu_3\text{-}O)\}^{6+}$ units linked through the two μ_4-O^{2-} ions.

The peripheral ligation in **3** is completed by two chelate NO$_3^-$ ions and two terminal MeOH molecules. All the metal ions are six-coordinate displaying distorted octahedral geometry. The Mn oxidation states and the protonation level of the O^{2-} ions were confirmed by charge balance considerations and bond-valence sum (BVS) calculations [39], as well as the observation of Jahn–Teller distortions at the Mn^{III} ions.

Closer inspection of the crystal structure of **3** reveals that there are no strong inter- or intramolecular interaction thus, the Mn_8 units are well-separated with the shortest metal⋯metal distance between neighboring molecules in **3** being 10.008 Å (Mn3⋯Mn4).

3 is a new addition in the small family of high nuclearity Mn/(py)C(ph)NO(H), which include Mn_3, Mn_4, Mn_6, Mn_8, Mn_{12} species [45,49–55]; it is the only one, among the latter, that display a $\{Mn_4^{II}Mn_4^{III}(\mu_4\text{-}O)_2(\mu_3\text{-}O)_2\}^{12+}$ double-butterfly structural core, although this topology is known in 3d metal cluster chemistry.

3.3. Magnetism studies

Solid state, variable-temperature magnetic susceptibility measurements were performed on vacuum-dried microcrystalline samples of complexes **1** and **2·3H_2O** suspended in eicosane to prevent torquing. The dc molar magnetic susceptibility (χ_M) data were collected in the 5.0–300 K range in a 0.1 T (1000 Oe) magnetic field, and are shown in Fig. 4 as $\chi_M T$ versus T plots. For **1**, the $\chi_M T$ steadily decreases with decreasing temperature from 5.11 cm^3 mol^{-1} K at 300 K to 2.73 cm^3 mol^{-1} K at 50 K and then drops rapidly to 0.71 cm^3 mol^{-1} K at 5.0 K. The $\chi_M T$ at 300 K is very close to the spin-only (g = 2) value of 5.0 cm^3 mol^{-1} K expected for one Mn^{III} and two Ni^{II} non-interacting ions. For **2·3H_2O**, the $\chi_M T$ value at 300 K is 7.54 cm^3 K mol^{-1}, close to the calculated one (8.0 cm^3 mol^{-1} K) for two Mn^{III} and two Ni^{II} non-interacting ions and decreases steadily with decreasing temperature to 0.56 cm^3 K mol^{-1} at 5.0 K. Clearly, the profiles of the $\chi_M T$ versus T plots for **1** and **2·3H_2O** reveal the existence of antiferromagnetic interactions between the metal ions and an $S = 0$ ground state.

The isotropic Heisenberg spin Hamiltonian for the linear complex **1** is given by Eq. (4), where J is the Ni^{II}–Mn^{III} and J' the Ni^{II}–Ni^{II} exchange interactions (Fig. 5):
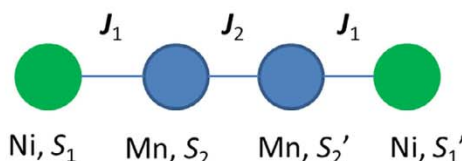
Scheme 3. Schematic representation of the coupling scheme used to model dc data for **2**.

$$\mathcal{H} = -2j\left(\hat{S}_1 \cdot \hat{S}_2 + \hat{S}_1 \cdot \hat{S}_{2'}\right) - 2J'\hat{S}_2 \cdot \hat{S}_2 \tag{4}$$

The distance between the Ni^{II} ions in **1** is 7.0(2) Å, hence the J' value is expected to be negligible and can be omitted from Eq. (4); the Hamiltonian is then simplified to

$$\mathcal{H} = -2j\left(\hat{S}_1 \cdot \hat{S}_2 + \hat{S}_1 \cdot \hat{S}_{2'}\right) \tag{5}$$

and its eigenvalues are given by Eq. (6), where $\hat{S}_A = \hat{S}_2 + \hat{S}_{2'}$, $S_1 = 2$ and $S_2 = S_{2'} = 1$, and S_T is the total spin of the whole molecule.

$$E(S_T, S_A) = -J[S_T(S_T + 1) - S_A(S_A + 1)] \tag{6}$$

Fitting of the experimental data for **1** to the corresponding Van Vleck equation [56] gave the solid line in Fig. 4, with fit parameters $J = -6.34 \pm 0.14$ cm^{-1} and $g = 2.09 \pm 0.01$, and a temperature-independent paramagnetism (TIP) term held constant at 300×10^{-6} cm^3 mol^{-1}.

The magnetic properties of **2·3H_2O** are modeled by the Hamiltonian equation $H = -2J_1 (\hat{S}_1 \cdot \hat{S}_2 + \hat{S}_1 \cdot \hat{S}_{2'}) - 2J_2 \hat{S}_2 \cdot \hat{S}_{2'}$ (7), according to Scheme 3. With this model and using the PHI software, the dc data were simulated with the obtained converging parameters being $J_1 = -4.57 \pm 0.08$ cm^{-1}, $J_2 = -12.72 \pm 0.12$ cm^{-1} and g = 2.18 ± 0.01 [57].

In order to independently probe the spin ground state value of **1** and **2·3H_2O**, alternating current (ac) magnetic susceptibility measurements were performed in the 2–15 K temperature range in a 3.5 Oe ac field oscillating at 50–950 Hz. Ac susceptibility studies are a powerful complement to dc studies for determining the ground state of a system, because they preclude any complications arising from the presence of a dc field. The $\chi'_M T$ for both compounds (Figs. S1 and S2 in Supplementary Material) decreases continuously with decreasing temperature, heading to zero 0 K, confirming their diamagnetic ground state.

4. Conclusions

Two mixed-metal, [Ni$_2^{II}$Mn^{III}{(py)C(Me)NO}$_6$](ClO$_4$) (**1**) and [Ni$_2^{II}$Mn$_2^{III}${(py)C(Me)NO}$_6$(OMe)$_2$(MeOH)$_2$](ClO$_4$)$_2$ (**2**), and one homometallic, [Mn$_4^{II}$Mn$_4^{III}$O$_4$(NO$_3$)$_2${(py)C(ph)NO}$_8$(HCO$_2$)$_2$(MeOH)$_2$] (**3**), compounds have been synthesized by the employment of 2-pyridyl oximes in Ni/Mn chemistry in the absence of auxiliary bridging ligands. **1** and **2** possess a linear and *zig-zag* metal arrangement, respectively, and are the first 3d–3d′ metal clusters, containing (py)C(Me)NOH. **3** displays a double-butterfly $\{Mn_4^{II}Mn_4^{III}(\mu_4\text{-}O)_2(\mu_3\text{-}O)_2\}^{12+}$ structural core and joins the small family of Mn/(py)C(ph)NO$^-$ complexes [45,49–55]. It is noteworthy to mention that the synthesis of **3** was inspired by the unsuccessful attempts to obtain new products by using small amounts of Ni(II) in the reaction system that gave compounds **1** and **2**. **1** and **2** have a diamagnetic ground state.

2-Pyridyl oximes have been extensively used in 3d and 3d-4f metal cluster chemistry and yielded compounds with interesting structures and extraordinary magnetic properties [20,21,30–35]. Their employment in 3d–3d′ metal chemistry, though, has not been systematically investigated, and this work demonstrates its potential to provide access to new compounds. We believe that
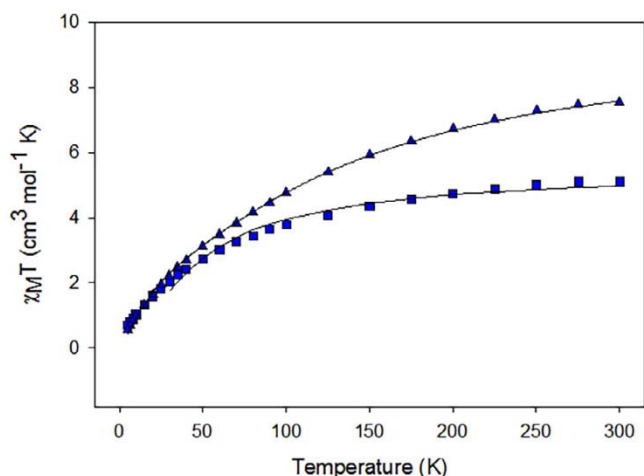
Fig. 4. $\chi_M T$ versus T plots for complexes **1** (■), and **2·3H_2O** (▲) in the temperature range 5.0–300 K in 0.1 T applied dc field. The solid lines represent the fit of the data to a theoretical expression; see the text for the fit parameters.
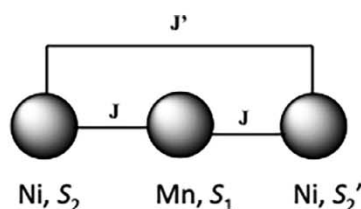
Fig. 5. The exchange interactions in **1**.

we have seen only the tip of the iceberg and further studies towards this direction are currently in progress, which will be reported in due course.

Acknowledgements

Appendix A. Supplementary data

CCDC contains 1913357–1913359 the supplementary crystallographic data for **1**–**3**. These data can be obtained free of charge via http://www.ccdc.cam.ac.uk/conts/retrieving.html, or from the Cambridge Crystallographic Data Centre, 12 Union Road, Cambridge CB2 1EZ, UK; fax: (+44) 1223-336-033; or e-mail: deposit@ccdc.cam.ac.uk. Supplementary data to this article can be found online at https://doi.org/10.1016/j.poly.2019.07.024.

References

[1] J. Fielden, L. Cronin, Coordination clusters, Encyclopedia of Supermolecular Chemistry, Taylor & Francis, 2005.
[2] C. Papatriantafyllopoulou, E.E. Moushi, G. Christou, A.J. Tasiopoulos, Chem. Soc. Rev. 45 (2016) 1597.
[3] G.E. Kostakis, S.P. Perlepes, V.A. Blatov, D.M. Proserpio, A.K. Powell, Coord. Chem. Rev. 256 (2012) 1246.
[4] (a) W. Schmitt, M. Murugesu, J.C. Goodwin, J.P. Hill, A. Mandel, R. Bhalla, C.E. Anson, S.L. Heath, A.K. Powell, Polyhedron 20 (2001) 1687;
(b) K.J. Mitchell, K.A. Abboud, G. Christou, Nature Commun. 8 (2017) 1445;
(c) A.E. Thuijs, X.-G. Li, Y.-P. Wang, K.A. Abboud, X.-G. Zhang, H.-P. Cheng, G. Christou, Nat. Commun. 8 (2017) 500.
[5] R. Bagai, G. Christou, Chem. Soc. Rev. 38 (4) (2009) 1011 (and references cited therein).
[6] G. Christou, D. Gatteschi, D.N. Hendrickson, R. Sessoli, MRS Bull. 25 (2000) 66.
[7] D. Gatteschi, R. Sessoli, Angew. Chem., Int. Ed. 42 (2003) 268.
[8] Z.-M. Zhang, L.-Y. Pan, W.-Q. Lin, J.-D. Leng, F.-S. Guo, Y.-C. Chen, J.-L. Liu, M.-L. Tong, Chem. Commun. 49 (2013) 8081.
[9] J.-D. Leng, J.-L. Liu, M.-L. Tong, Chem. Commun. 48 (2012) 5286.
[10] J.-B. Peng, Q.-C. Zhang, X.-J. Kong, Y.-P. Ren, L.-S. Long, R.-B. Huang, L.-S. Zheng, Z. Zheng, Angew. Chem., Int. Ed. 50 (2011) 10649.
[11] E.C. Theila, R.K. Behera, T. Tosha, Coord. Chem. Rev. 257 (2013) 579.
[12] K.L. Taft, G.C. Papaefthymiou, S.J. Lippard, Science 259 (1993) 1302.
[13] B. Loll, J. Kern, W. Saenger, A. Zouni, J. Biesiadka, Nature 438 (2005) 1040.
[14] K. Sauer, J. Yano, V.K. Yachandra, Coord. Chem. Rev. 252 (2008) 318.
[15] P. Chaudhuri, Coord. Chem. Rev. 243 (2003) 143.
[16] A.J.L. Pombeiro, V. Yu Kukushkin, in: J.A. McCleverty, T.J. Meyer (Eds.), Comprehensive Coordination Chemistry II, vol. 7, Elsevier, Amsterdam, 2004, pp. 631–637.
[17] C.J. Milios, S. Piligkos, E.K. Brechin, Dalton Trans. (2008) 1809 (Perspective).
[18] C.J. Milios, A. Vinslava, W. Wernsdorfer, S. Moggach, S. Parsons, S.P. Perlepes, G. Christou, E.K. Brechin, J. Am. Chem. Soc. 129 (2007) 2754.
[19] L.F. Jones, A. Prescimone, M. Evangelisti, E.K. Brechin, Chem. Commun. (2009) 2023.
[20] C. Papatriantafyllopoulou, L.F. Jones, T.D. Nguyen, N. Matamoros-Salvador, L. Cunha-Silva, F.A. Almeida Paz, J. Rocha, M. Evangelisti, E.K. Brechin, S.P. Perlepes, Dalton Trans. (2008) 3153.
[21] C.G. Efthymiou, L. Cunha-Silva, S.P. Perlepes, E.K. Brechin, R. Inglis, M. Evangelisti, C. Papatriantafyllopoulou, Dalton Trans. 45 (2016) 17409.
[22] G. Rogez, J.-N. Rebilly, A.-L. Barra, L. Sorace, G. Blondin, N. Kirchner, M. Duran, J. van Slageren, S. Parsons, L. Ricard, A. Marvilliers, T. Mallah, Angew. Chem., Int. Ed. 44 (2005) 1876.
[23] M. Charalambous, E.E. Moushi, C. Papatriantafyllopoulou, W. Wernsdorfer, V. Nastopoulos, G. Christou, A.J. Tasiopoulos, Chem. Commun. 48 (2012) 5410.
[24] L. Martinez, J.S. Gancheff, F.E. Hahn, R.A. Burrow, R. Gonzalez, C. Kremer, R. Chiozzone, Spectrochim. Acta A 105 (2013) 439.
[25] (a) Rigaku Oxford Diffraction (2015). CrysAlisPRO (version 1.171.38.43). Rigaku Oxford Diffraction, Yarnton, UK.;
(b) G.M. Sheldrick, Acta Crystallogr., Sect A 71 (2015) 3.
[26] L.J. Farrugia, J. Appl. Crystallogr. 45 (2012) 849.
[27] K. Brandenburg, DIAMOND. Version 3.1d. Crystal Impact GbR, Bonn, Germany, 2006.
[28] C.F. Macrae, P.R. Edgington, P. McCabe, E. Pidcock, G.P. Shields, R. Taylor, M. Towler, J. Van de Streek, J. Appl. Crystallogr. 39 (2006) 453.
[29] A.L. Spek, Acta Crystallogr., Sect. C 71 (2015) 9.
[30] For a comprehensive review, see: C.J. Milios, T.C. Stamatatos, S.P. Perlepes, Polyhedron 25 (2006) 134 (Polyhedron Report).
[31] C. Papatriantafyllopoulou, T.C. Stamatatos, C.G. Efthymiou, L. Cunha-Silva, F.A. Paz, S.P. Perlepes, G. Christou, Inorg. Chem. 49 (2010) 9743.
[32] T.C. Stamatatos, A. Escuer, K.A. Abboud, C.P. Raptopoulou, S.P. Perlepes, G. Christou, Inorg. Chem. 47 (2008) 11825.
[33] T.C. Stamatatos, K.A. Abboud, S.P. Perlepes, G. Christou, Dalton Trans. (2007) 3861.
[34] S. Zhang, L. Zhen, B. Xu, R. Inglis, K. Li, W. Chen, Y. Zhang, K.F. Konidaris, S.P. Perlepes, E.K. Brechin, Y. Li, Dalton Trans. (2010) 3563.
[35] T.C. Stamatatos, C. Papatriantafyllopoulou, E. Katsoulakou, C.P. Raptopoulou, S. P. Perlepes, Polyhedron 26 (2007) 1830.
[36] B. Biswas, S. Khanra, T. Weyhermüller, P. Chaudhuri, Chem. Commun. (2007) 1059.
[37] S.Y. Nurova, E.P. Turevskaya, V.G. Kessler, M.I. Yanovskaya, The Chemistry of Metal Alkoxides, Kluwer AP, Dordrecht, 2002.
[38] A.J. Tasiopoulos, S.P. Perlepes, Dalton Trans. (2008) 5537.
[39] W. Liu, H.H. Thorp, Inorg. Chem. 32 (1993) 4102.
[40] H. Chen, C.-B. Ma, D.-Q. Yuan, M.-Q. Hu, H.-M. Wen, Q.-T. Liu, C.-N. Chen, Inorg. Chem. 50 (2011) 10342.
[41] R. Clerac, H. Miyasaka, M. Yamashita, C. Coulon, J. Am. Chem. Soc. 124 (2002) 12837.
[42] H. Miyasaka, T. Nezu, K. Sugimoto, K. Sugiura, M. Yamashita, R. Clerac, Chem. Eur. J. 11 (2005) 1592.
[43] H. Miyasaka, T. Nezu, F. Iwahori, S. Furukawa, K. Sugimoto, R. Clerac, K. Sugiura, M. Yamashita, Inorg. Chem. 42 (2003) 4501.
[44] Y. An, B. Yuan, J. Tao, A.-L. Cui, H.-Z. Kou, Inorg. Chim. Acta 387 (2012) 401.
[45] D.I. Alexandropoulos, M.J. Manos, C. Papatriantafyllopoulou, S. Mukherjee, A.J. Tasiopoulos, S.P. Perlepes, G. Christou, T.C. Stamatatos, Dalton Trans. 41 (2012) 4744.
[46] P. Chaudhuri, T. Weyhermuller, R. Wagner, S. Khanra, B. Biswas, E. Bothe, E. Bill, Inorg. Chem. 46 (2007) 9003.
[47] T. Weyhermuller, R. Wagner, S. Khanra, P. Chaudhuri, Dalton Trans. (2005) 2539.
[48] G. Psomas, A.J. Stemmler, C. Dendrinou-Samara, J.J. Bodwin, M. Schneider, M. Alexiou, J.W. Kampf, D.P. Kessissoglou, V.L. Pecoraro, Inorg. Chem. 40 (2001) 1562.
[49] M. Holynska, J. Klak, Z. Kristallogr Cryst. Mater. 227 (2012) 635.
[50] C.C. Stoumpos, R. Inglis, O. Roubeau, H. Sartzi, A.A. Kitos, C.J. Milios, G. Aromi, A.J. Tasiopoulos, V. Nastopoulos, E.K. Brechin, S.P. Perlepes, Inorg. Chem. 49 (2010) 4388.
[51] C.J. Milios, S. Piligkos, A.R. Bell, R.H. Laye, S.J. Teat, R. Vicente, E. McInnes, A. Escuer, S.P. Perlepes, R.E.P. Winpenny, Inorg. Chem. Commun. 9 (2006) 638.
[52] M. Holynska, S. Dehnen, Inorg. Chem. Commun. 14 (2011) 1290.
[53] T.C. Stamatatos, D. Foguet-Albiol, C.C. Stoumpos, C.P. Raptopoulou, A. Terzis, W. Wernsdorfer, S.P. Perlepes, G. Christou, Polyhedron 26 (2007) 2165.
[54] C.J. Milios, E. Kefalloniti, C.P. Raptopoulou, A. Terzis, R. Vicente, N. Lalioti, A. Escuer, S.P. Perlepes, Chem. Commun. (2003) 819.
[55] C.J. Milios, T.C. Stamatatos, P. Kyritsis, A. Terzis, C.P. Raptopoulou, R. Vicente, A. Escuer, S.P. Perlepes, Eur. J. Inorg. Chem. (2004) 2885.
[56] J.H. Van Vleck, The Theory of Electric and Magnetic Susceptibilities, Oxford Press, London, 1932.
[57] N.F. Chilton, R.P. Anderson, L.D. Turner, A. Soncini, K.S. Murray, J. Comput. Chem. 34 (2013) 1164.